Structural Monitoring and Maintenance, *Vol. 5, No. 1 (2018) 15-38*
DOI: https:// doi.org/10.12989/smm.2018.5.1.015

Nonlinear impact of negative stiffness dampers on stay cables

Xiang Shi[1,2a] and Songye Zhu[*2]

[1]*College of Information and Control Engineering, China University of Petroleum (East China), Qingdao 266580, Shandong Province, China*
[2]*Department of Civil and Environmental Engineering, The Hong Kong Polytechnic University, Kowloon, Hong Kong, China*

(Received November 15, 2017, Revised February 11, 2018, Accepted February 18, 2018)

Abstract. Negative stiffness dampers (NSDs) have been proven an efficient solution to vibration control of stay cables. Although previous studies usually assumed a linear negative stiffness behavior of NSDs, many negative stiffness devices produce negative stiffness with nonlinear behavior. This paper systematically evaluates the impact of nonlinearity in negative stiffness on vibration control performance for stay cables. A linearization method based on energy equivalent principle is proposed, and subsequently, the impact of two types of nonlinear stiffness, namely, displacement hardening and softening stiffness, is evaluated. Through the Hilbert transform (HT) of free vibration responses, the effects of nonlinear stiffness of an NSD on the modal frequencies, damping ratios and frequency response functions of a stay cable is also investigated. The HT analysis results validate the accuracy of the linearization method.

Keywords: nonlinear negative stiffness; stay cable; vibration control; linearization

1. Introduction

As widely used important load-carrying elements in bridges, stay cables are often susceptible to unexpectedly large oscillations under dynamic loads due to their high flexibility and low inherent damping (Yamaguchi and Fujino 1998). Extensive research works have been carried out in the past two decades on suppressing stay cable vibrations using various vibration control approaches, including passive dampers (Kovacs 1982, Pacheco *et al.* 1993, Krenk 2000, Main and Jones 2002a, 2002b, Spencer and Nagarajaiah 2003, Krenk and Høgsberg 2005, Fujino and Hoang 2008, Hoang and Fujino 2009), semi-active dampers (Johnson *et al*. 2003, Ni *et al.* 2002, Christenson *et al*. 2006, Chen *et al*. 2015; Li *et al*. 2005, Wu and Cai 2006, Zhou and Sun 2013), and active dampers (Li *et al.* 2008). Among them, passive dampers have been most widely implemented in real applications; however, when installed close to cable anchorages, passive dampers only add limited damping to stay cables. In comparison, semi-active and active control techniques have been proven higher performance solutions for vibration control of stay cables.

Moreover, some past studies on active control have revealed that an interesting control behavior with apparent negative-stiffness force–deformation relationship may benefit control

∗Corresponding author, Ph.D., E-mail: ceszhu@polyu.edu.hk
[a] Ph.D., Email: chnxshi@gmail.com

http://www.techno-press.org/?journal=smm&subpage=7 ISSN: 2288-6605 (Print), 2288-6613 (Online)

performance in some situations, including in vibration mitigation of stay cables (Iemura and Pradono 2002, Li *et al.* 2008). Therefore, a variety of semi-active or passive negative stiffness dampers (NSDs) were developed to imitate similar hysteresis of active control. For example, Weber and Boston (2011) designed semi-active magnetorheological (MR) dampers to demonstrate negative stiffness behavior. In addition, several representative examples of passive NSDs were proposed based on pre-buckled beams (Lee *et al.* 2007), pre-compressed springs (Pasala *et al.* 2013), sliding pendulum with a convex friction interface (Iemura and Pradono, 2009). In particular, Shi and Zhu (2015, 2017) recently proposed and developed two magnetic NSD (MNSD) designs that efficiently integrate magnetic negative-stiffness mechanism and eddy-current damping in compact cylindrical configurations. Compared with active and semi-active counterparts, passive NSDs do not require power supply and feedback systems.

The effectiveness of using semi-active and passive NSDs for stay cable vibration control has been successfully demonstrated in the past literature (Webber and Boston 2011, Weber and Distl 2015, Shi *et al*. 2016, Zhou and Li 2016, Shi *et al.* 2017a, Shi *et al.* 2017b). Shi *et al*. (2016) present the first analytical study on the dynamic behavior of a taut cable with an NSD and found that asymptotic solution loses its accuracy when an NSD possesses highly negative stiffness. Later, Shi *et al.* (2017a) experimentally verified that a passive MNSD can offer a damping ratio four times as large as that added by a conventional viscous damper. Zhou and Li (2016) demonstrate good control performance of another type of NSD made of pre-stressed springs plus oil dampers. A recent comparative study indicated passive linear NSD can provide control performances comparable to active controllers (Shi *et al.* 2017b).

Therefore, passive NSDs certainly present a preferred solution to stay cable vibration control by considering their simplicity and practicability. To maximize the damping ratio of a stay cable, each negative stiffness coefficient corresponds to an optimal damping coefficient (Shi *et al.* 2016). However, many passive NSDs exhibit nonlinear negative stiffness, which makes the optimal tuning of damping coefficients difficult. The impact of nonlinearity in negative stiffness has not been examined for stay cable vibration control. Therefore, this paper systematically evaluates the effect of nonlinear negative stiffness (including both softening and hardening stiffness) of NSDs when applied to stay cables. A linearization method based on energy equivalent principle is proposed. Based on this method, the influences of the stiffness nonlinearity are analyzed for both hardening and softening negative stiffness. The impacts of the nonlinear negative stiffness on the modal frequencies, damping ratios and frequency response functions (FRF) of the stay cable are also investigated via Hilbert transform (HT) of the free vibration response of a stay cable with a nonlinear NSD. The results from the HT analysis validate the accuracy of the linearization method.

2. Dynamic formulation for stay cables

Fig. 1 shows a schematic drawing of a stay cable with length L, tension T, mass per unit length m, and flexural rigidity EI. A control device is installed in the transverse direction at a close distance a from the left end of the cable. The distance from the control device to the right end is $a'=L-a$. In practice, a is often limited within the range of 2-5% of the total length L. The transverse vibration of an uncontrolled stay cable subjected to external excitations is described by the following differential equation:

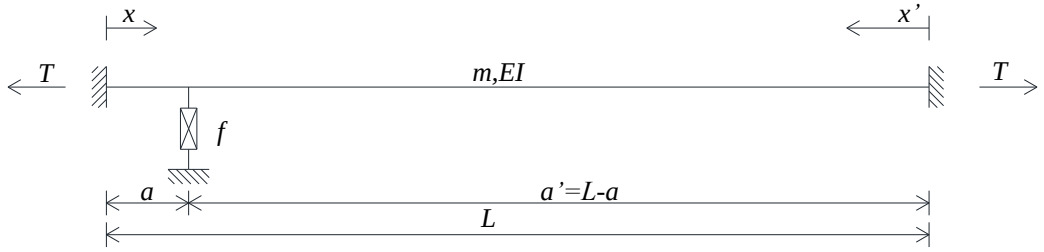

Fig. 1 A stay cable considering flexural rigidity with a passive NSD at $x=a$

$$T\frac{\partial^2 u}{\partial x^2}-\frac{\partial^2}{\partial x^2}\left(EI\frac{\partial^2 u}{\partial x^2}\right)-c\frac{\partial u}{\partial t}-m\frac{\partial^2 u}{\partial t^2}=w(x,t) \tag{1}$$

where $u(x,t)$ is the transverse displacement at location x and instant t, $w(x,t)$ is the external excitation at location x and instant t. Both ends are assumed to be fixed, i.e., $u(0,t)=u(L,t)=u'(0,t)=u'(L,t)=0$. The effect of flexural rigidity of stay cable is considered in Eq. (1) in this paper.

The dynamic model built in this paper is based on the finite difference model proposed by Mehrabi and Tabatabai (1998). The original model was normalized with respect to the discretized element length. They are modified slightly in this paper to obtain absolute responses instead of the normalized ones. The same model was also employed in the previous studies done by the authors (e.g., Shi *et al.* 2017b). The stiffness matrix of an uncontrolled stay cable with a uniform cross section can be expressed as

$$\mathbf{K}=\begin{bmatrix} Q & D & W & & & 0 \\ D & S & D & W & & \\ W & D & S & D & \ddots & \\ & W & \ddots & \ddots & \ddots & W \\ & & \ddots & \ddots & S & D \\ 0 & & & W & D & Q \end{bmatrix} \tag{2a}$$

where

$$S=\frac{6EI}{l^3}+\frac{2T}{l} \tag{2b}$$

$$D=-\frac{4EI}{l^3}-\frac{T}{l} \tag{2c}$$

$$W=\frac{EI}{l^3} \tag{2d}$$

and Q depends on the boundary conditions. For fixed end conditions at both ends

$$Q = \frac{7EI}{l^3} + \frac{2T}{l} \tag{2e}$$

for pinned end condition at both ends

$$Q = \frac{5EI}{l^3} + \frac{2T}{l} \tag{2f}$$

where $l = L/(n+1)$ is the discretized element length of the cable; n is the number of node and n+1 is the number of elements; and EI is constant along the cable.

Accordingly, the mass matrix can be expressed using the lumped mass model

$$\mathbf{M} = \mathbf{I_n} \cdot ml \tag{3}$$

where m is mass per unit length that is constant along the whole cable. The damping matrix **C** can be constructed according to Rayleigh damping.

The matrix form of a stay cable with external excitation is

$$\mathbf{M\ddot{u}} + \mathbf{C\dot{u}} + \mathbf{Ku} = \mathbf{w} \tag{4}$$

where **u** and **w** are the displacement and load vectors

$$\mathbf{u} = \begin{bmatrix} u_1 & u_2 & \dots & u_n \end{bmatrix}^T \tag{5}$$

$$\mathbf{w} = \begin{bmatrix} w_1 & w_2 & \dots & w_n \end{bmatrix}^T \tag{6}$$

where u_i is the displacement of the i_{th} node and w_i is the external force on the i^{th} node.

The equation of motion (i.e., Eq. (4)) can be converted to state space representation as

$$\dot{\mathbf{z}} = \mathbf{Az} + \mathbf{B_w w} \tag{7}$$

where **z** is the state vector

$$\mathbf{z} = \begin{bmatrix} \mathbf{u} \\ \dot{\mathbf{u}} \end{bmatrix} \tag{8}$$

A is the state matrix,

$$\mathbf{A} = \begin{bmatrix} \mathbf{0} & \mathbf{I} \\ \mathbf{-M^{-1}K} & \mathbf{-M^{-1}C} \end{bmatrix} \tag{9}$$

$\mathbf{B_w}$ is the input matrix for excitation forces

$$\mathbf{B_w} = \begin{bmatrix} \mathbf{0} \\ \mathbf{M^{-1}} \end{bmatrix} \tag{10}$$

The complex modal frequencies and mode shapes can be obtained by eigenvalue analysis of the state matrix **A**. The continuous state space model in Eq. (7) can be converted to a discrete model using z-transform and the response time histories of the stay cable can be conveniently computed.

3. Modeling of Nonlinear NSD

A taut cable installed with a nonlinear viscous damper has been systematically studied in the past (Main and Jones 2002b, Krenk and Høgsberg 2005, Hoang and Fujino 2009). A force-velocity relation of a nonlinear viscous damper is usually described by a power law form

$$f_c\left(\dot{u}(a,t)\right) = c_n \dot{u}(a,t)^{\alpha} \tag{11}$$

where $f_c\left(\dot{u}(a,t)\right)$ is the viscous damping force, c_n is the damping coefficient of the nonlinear viscous damper, $\dot{u}(a,t)$ is the cable velocity at the damper location, and α is the power coefficient describing the nonlinearity. The corresponding force-velocity relationships for α <1, α =1 and α >1 are illustrated schematically in Fig. 2. When α =1, the damping behavior is linear; when 0< α <1, the damping coefficient softens with the increasing damper velocity; when α >1, the damping coefficient hardens with the increasing damper velocity.

If such a power-law form is extended to describe the nonlinear negative stiffness force, we have

$$f_k\left(u(a,t)\right) = k_n u(a,t)^{\alpha} \tag{12}$$

where $f_k\left(u(a,t)\right)$ is the stiffness force, k_n is the stiffness coefficient of an NSD, $u(a,t)$ is the cable displacement at the damper location. When the coefficient α >1, it describes a displacement-hardening negative stiffness; when 0< α <1, it describes a displacement-softening negative stiffness. Accordingly, the tangent negative stiffness can be expressed as

$$k_{\mathrm{t}}\left(u(a,t)\right) = k_n \alpha u(a,t)^{\alpha-1} \tag{13}$$

The shortcoming of the power-law stiffness is apparent: when the damper displacement is zero, the tangent stiffness $k_{\mathrm{t}}(u(a,t))$ is zero if α >1 and is infinite if α < 1. It is certainly inconsistent with the actual situation.

Therefore, the method proposed by Nayfeh (1979) to simulate the behavior of nonlinear negative stiffness is adopted in this paper. A nonlinear force-displacement relationship can be expressed as an expansion of power series

$$\begin{aligned} f_k\left(u(a,t)\right) &= k_n\left(u(a,t)\right)u(a,t) \\ &= \left(\alpha_1 + \alpha_3 u(a,t)^2 + \alpha_5 u(a,t)^4 + \cdots\right)u(a,t) \\ &= \left(\sum_{n=1}^{N} \alpha_{2n-1} u(a,t)^{2n-2}\right)u(a,t) \end{aligned} \tag{14}$$

where $k_{\mathrm{n}}(u(a,t))$ is the nonlinear stiffness function with respect to $u(a,t)$, α_{2n-1} are coefficients and n=1,2,…,N.

Based on Eq. (14), the tangent stiffness k_{t} can be calculated as

$$k_{\mathrm{t}}\left(u(a,t)\right) = \sum_{n=1}^{N}(2n-1)\alpha_{2n-1} u(a,t)^{2n-2} \tag{15}$$

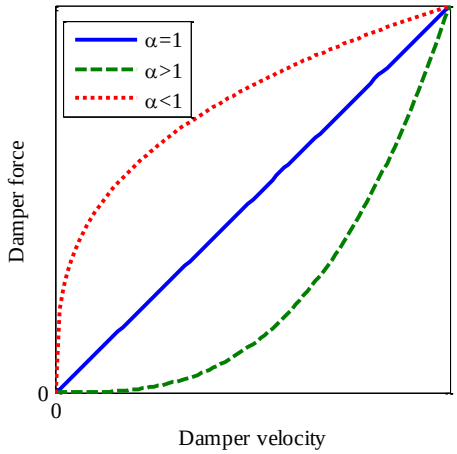

Fig. 2 Schematic force–velocity curves for power-law damper

When only the first term is used (i.e., *N*=1), Eq. (15) represents linear negative stiffness. When two power terms are used (i.e., *N*=2), Eq. (15) can describe nonlinear stiffness: α_1 defines the initial stiffness and α_3 defines the degree of nonlinearity. For example, $\alpha_1 \le 0$ and $\alpha_3 < 0$ describe the negative stiffness hardening with the increasing displacement; whereas $\alpha_1 < 0$ and $\alpha_3 > 0$ describe the negative stiffness softening with the increasing displacement. The nonlinear force displacement relationship is presented schematically in Fig. 3.

In order to avoid the instability of the stay cable caused by too large negative stiffness, the maximum tangent stiffness shall not exceed the following stability limit according to Shi *et al*. (2016)

$$\inf k_t = -\frac{l}{l-a} \cdot \frac{T}{a} \tag{16}$$

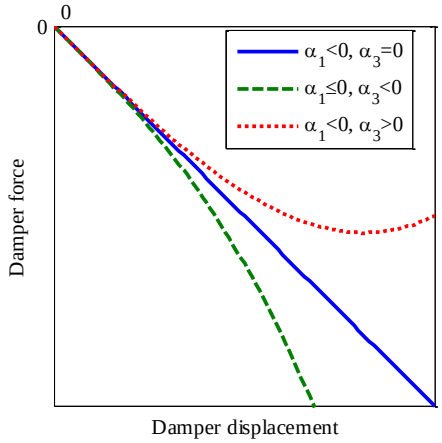

Fig. 3 Schematic force–displacement curves for power-series damper

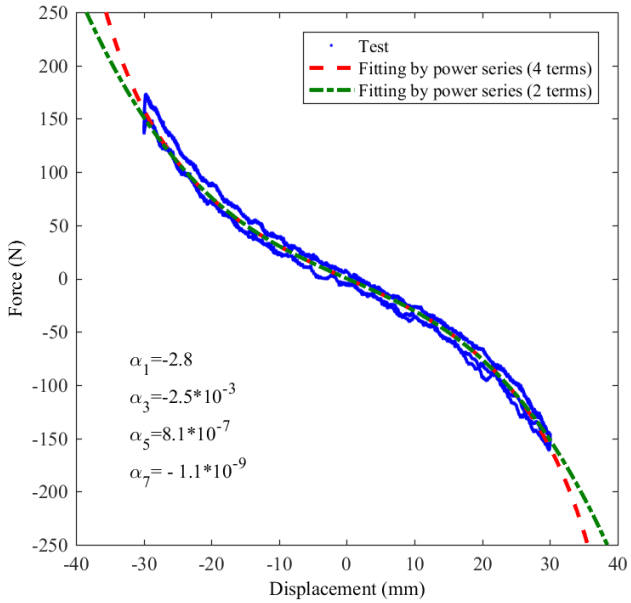

Fig. 4 Fitting damper force of MNSD-A with power series expansion

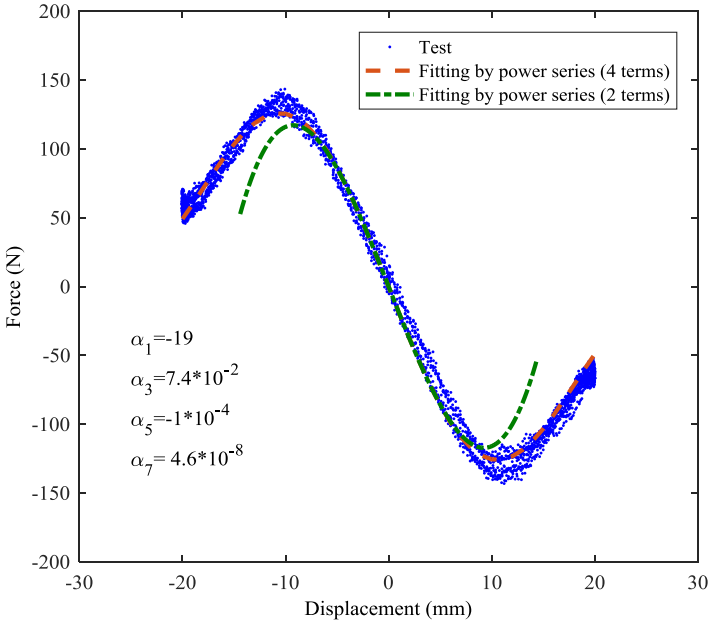

Fig. 5 Fitting damper force of MNSD-B with power series expansion

The maximum tangent stiffness k_t may occur at the zero and peak displacements in the softening and hardening types of NSDs, respectively. In this study, the negative stiffness is always constrained within the stability limit. Higher order terms of α_{2n-1} can be added to improve the modeling accuracy of nonlinear negative stiffness.

Two designs of MNSD invented by Shi and Zhu (2015, 2017), namely MNSD-A and MNSD-B, are chosen as examples, where the former and latter exhibit apparent hardening and softening stiffness behavior (Figs. 4 and 5), respectively. Figs. 4 and 5 shows the fitting effects of the adopted power-series model for the two considered MNSD-A and MNSD-B dampers, respectively, where a total of four power terms are used to model the damper force-displacement relationships and their corresponding values are shown in Figs. 4 and 5 as well. In general, the series of four power terms can describe the behavior of both MNSDs accurately. Although this study is based on the modeling of two MNSDs, it is believed that the conclusions from these representative NSDs can be generalized to other nonlinear NSDs for stay cable vibration control.

4. Linearization of nonlinear stiffness

Hoang and Fujino (2009) proposed a linearization approach when studying a nonlinear viscous damper subjected to harmonic vibration as follows with amplitude U_a and period T_n at damper location

$$u(a,t) = U_a \sin\left(\frac{2\pi}{T_n} t\right) \tag{17}$$

where U_a and T_n are the amplitude and period of the harmonic vibration at the damper location. Then, the nonlinear damping force can be approximated by the linearization

$$f_c\left(\dot{u}(a,t)\right) = c_n \dot{u}(a,t)^{\alpha} \approx c_e\left(U_a\right)\dot{u}(a,t) \tag{18}$$

where c_e represents an equivalent linear viscosity, which can be determined based on the energy equivalence principle (Krenk and Høgsberg 2005, Hoang and Fujino 2009)

$$c_e = \frac{\int_0^{T_n} f_c\left(\dot{u}(a,t)\right)\dot{u}(a,t)\,dt}{\int_0^{T_n} \dot{u}(a,t)^2\,dt} \tag{19}$$

Such an energy equivalent principle is extended in this paper to derive the equivalent linear stiffness from nonlinear negative stiffness behavior. Based on this principle, the nonlinear negative stiffness can be linearized to equivalent linear stiffness by equaling the energy required to restore the stiffness to certain displacement level

$$E_l = E_n \tag{20}$$

where E_l and E_n represent the strain energy of the systems with the linear and nonlinear stiffness, respectively

$$E_l = \int_0^{U_a} k_e u(a,t) du(a,t)_l = k_e \int_0^{U_a} u(a,t) du(a,t)$$
$$E_n = \int_0^{U_a} f_k(u(a,t)) du(a,t) = \int_0^{U_a} k_n(u(a,t)) u(a,t) du(a,t) \tag{21}$$

where k_e is the equivalent linear stiffness.

According to Eqs. (20) and (21), the equivalent stiffness k_e is dependent on the vibration amplitude and can be calculated by

$$k_e = \frac{\int_0^{U_a} k_n(u(a,t)) u(a,t) du(a,t)}{\int_0^{U_a} u(a,t) du(a,t)} \tag{22}$$

where

$$\int_0^{U_a} u(a,t) du(a,t) = \frac{1}{2} U_a^2 \tag{23}$$

and

$$\begin{aligned} &\int_0^{U_a} k_n(u(a,t)) u(a,t) du(a,t) \\ &= \int_0^{U_a} (\alpha_1 + \alpha_3 u_a^2 + \alpha_5 u_a^4 + \cdots) u(a,t) du(a,t) \\ &= \left(\frac{1}{2}\alpha_1 U_a + \frac{1}{4}\alpha_3 U_a^3 + \frac{1}{6}\alpha_5 U_a^5 + \cdots \right) U_a \\ &= \sum_{n=1}^{N} \frac{1}{2n} \alpha_{2n-1} U_a^{2n} \end{aligned} \tag{24}$$

As a result, the equivalent stiffness k_e is expressed as

$$k_e(U_a) = \frac{\sum_{n=1}^{N} \frac{1}{2n} \alpha_{2n-1} U_a^{2n}}{\frac{1}{2} U_a^2} = \sum_{n=1}^{N} \frac{1}{n} \alpha_{2n-1} U_a^{2n-2} \tag{25}$$

The equivalent stiffness k_e is an important parameter to evaluate the performance of a nonlinear stiffness damper with respect to vibration amplitudes in a given period. Meanwhile, the tangent stiffness k_t shall be kept below the stability limit in Eq. (16) at any instant.

Given the coefficients α_{2n-1} shown in Fig. 4, the equilvalent and tangent stiffness can be calculated based on Eq. (25) and Eq. (15), respectively. Figs. 6(a) and 6(b) show the tangent and equivalent linear stiffneses of MNSD-A, respectively, by considering different numbers of terms in the power series. The modeling accuracy will be improved as more terms are included in the power series. However, the nonlinearity in the equivalent stiffness is much smaller than that in the tangent stiffness. The contribution of the lower terms on the equilvaent stiffness is more than the higher terms. In general, the first two terms are sufficient to well describe the damper force and the hardening behavior of the equivalent stiffness in MNSD-A, as shown in Fig. 6(b).

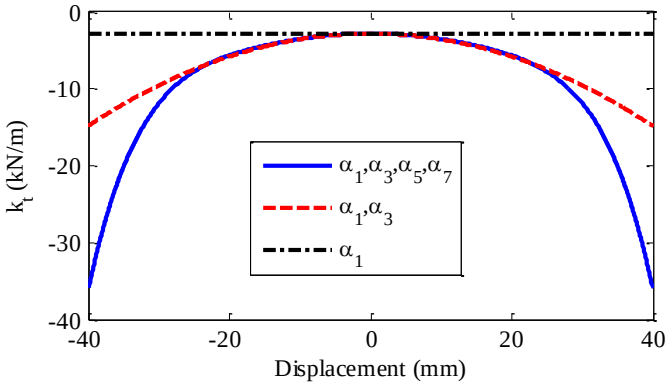

(a) Tangent stiffness

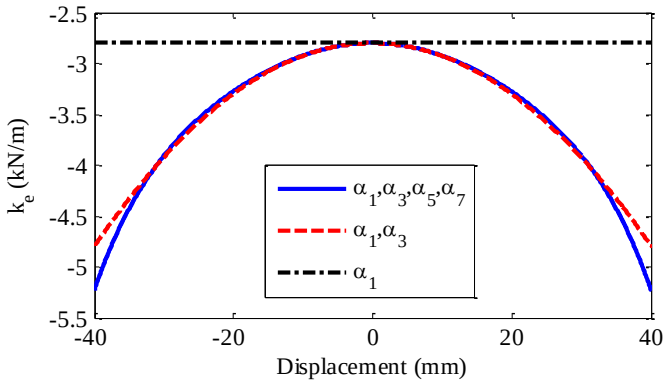

(b) Equivalent stiffness

Fig. 6 Negative stiffness of MNSD-A

Similar observation can be made to the MNSD-B with stiffness softening behavior. Figs. 7(a) and 7(b) show the tangent and equiavlent stiffneses of MNSD-B, respectively, corresponding to the coefficients α_{2n-1} shown in Fig. 5. In general, the first two terms can well descrbe the damper force and the softening behavior of the tangent and equivalent stiffness in MNSD-B, as shown in Figs. 5 and 7, respectively. The nonlinearity of the tangent stiffness with the increasing displacment is much larger than that of the equivalent stiffness.

Since the first two terms in the power series can reasonably simulate the nonlinear (either hardening or softening) negative stiffness of MNSDs, only these two terms are considered hereinafter in this paper. Consequently, Eqs. (15) and (25) for the tangent and equivalent stiffness can be simplified as

$$k_{\mathrm{t}}\left(u(a,t)\right)=\alpha_1+3\alpha_3\left(u(a,t)\right)^2 \tag{26}$$

$$k_{\mathrm{e}}\left(U_a\right)=\alpha_1+\frac{1}{2}\alpha_3 U_a^2 \tag{27}$$

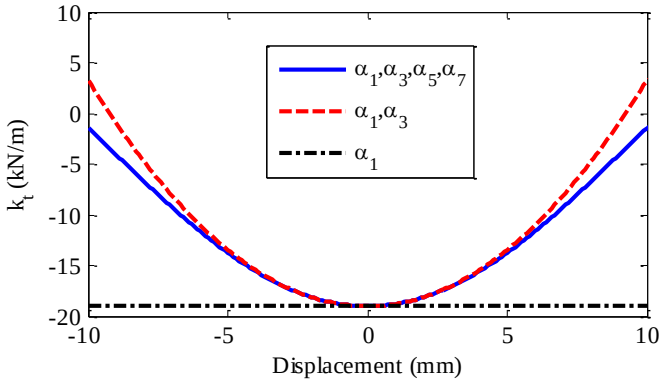

(a) Tangent stiffness

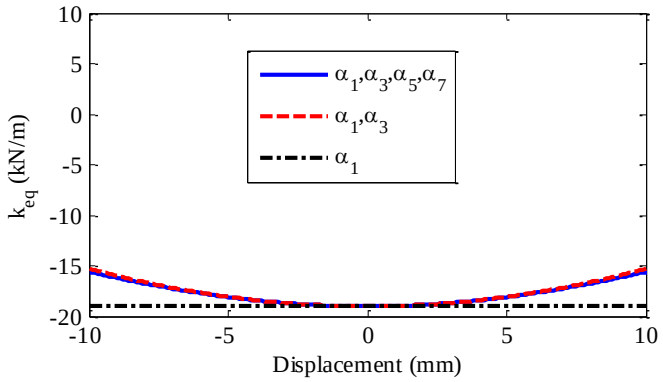

(b) Equivalent stiffness

Fig. 7 Negative stiffness of MNSD-B

4.1 Displacement hardening negative stiffness

$\alpha_1 \le 0$ and $\alpha_3 < 0$ should be adopted to simulate the negative stiffness that hardens with the increasing displacement. Instead of using the single set of the coefficients shown in Fig. 4, different combinations of α_1 and α_3 are used to consider different degrees of nonlinearity. Table 1 presents three cases with the varying α_1 and α_3 coefficients, which represent three cases with weak, medium, and strong nonlinearities in hardening negative stiffness. Fig. 8 shows the variation of the tangent and equivalent stiffness with the displacement amplitude in the three cases. In general, the equivalent stiffness shows less hardening with the displacement, compared with the tangent stiffness. It should be noted that in Fig. 8(a), the tangent stiffness in all three cases is always kept below the stability limit defined in Eq. (16).

4.2 Displacement Softening Negative Stiffness

$\alpha_1 < 0$ and $\alpha_3 > 0$ should be adopted to simulate the negative stiffness that softens with the

increasing displacement. Similarly, different combinations of α_1 and α_3 are considered to represent weak, medium, and strong nonlinearities in softening negative stiffness. The detailed parameters and the tangent stiffness at zero and maximum displacement are presented in Table 2. Fig. 9 shows the variation of the tangent and equivalent negative stiffness with the increasing displacement in the three cases. Again, the maximum negative stiffness (i.e., the initial stiffness) is always kept smaller than the stability limit presented in Eq. (16).

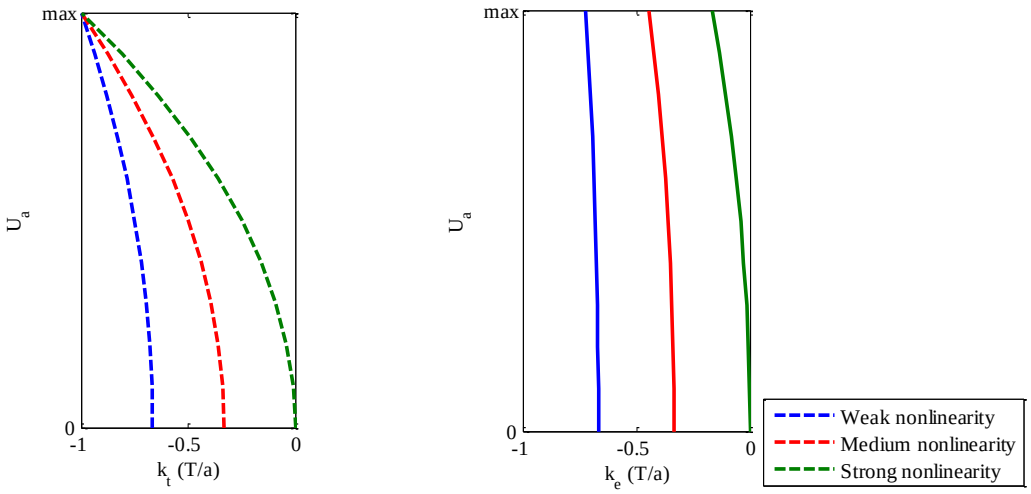

(a) Tangent stiffness (b) Equivalent stiffness

Fig. 8 Stiffness variation in the displacement hardening negative stiffness cases

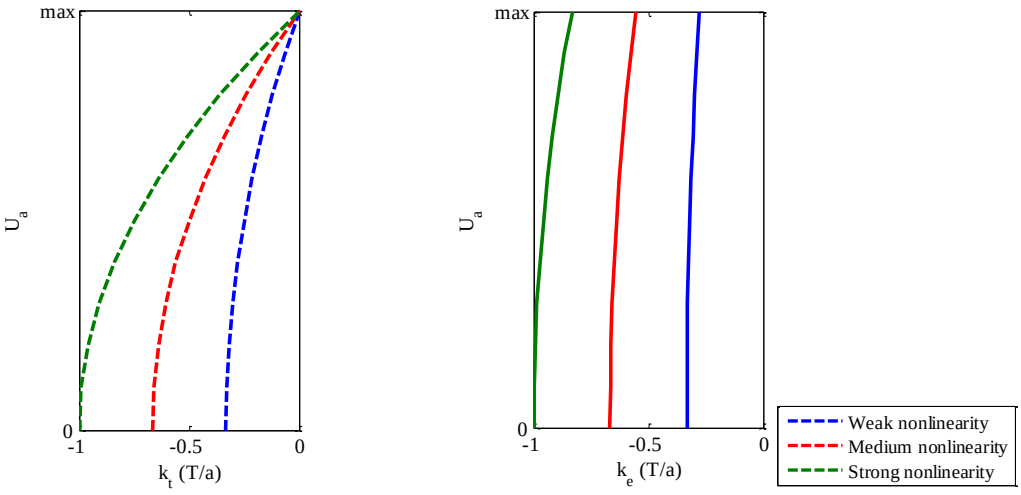

(a) Tangent stiffness (b) Equivalent stiffness

Fig. 9 Stiffness variation in the displacement softening negative stiffness cases

Table 1 Parameters of displacement hardening negative stiffness

Nonlinearity	α_1	α_3	$k_t(0)$	$k_t(U_{max})$
Weak	$-\frac{2}{3}\cdot\frac{T}{a}$	$-\frac{T}{3a}\cdot\frac{1}{3U_{max}^2}$	$-\frac{2}{3}\cdot\frac{T}{a}$	$-\frac{T}{a}$
Medium	$-\frac{1}{3}\cdot\frac{T}{a}$	$-\frac{2T}{3a}\cdot\frac{1}{3U_{max}^2}$	$-\frac{1}{3}\cdot\frac{T}{a}$	$-\frac{T}{a}$
Strong	0	$-\frac{T}{a}\cdot\frac{1}{3U_{max}^2}$	0	$-\frac{T}{a}$

Table 2 Parameters of displacement softening negative stiffness

Nonlinearity	α_1	α_3	$k_t(0)$	$k_t(U_{max})$
Weak	$-\frac{1}{3}\cdot\frac{T}{a}$	$\frac{T}{3a}\cdot\frac{1}{3U_{max}^2}$	$-\frac{1}{3}\cdot\frac{T}{a}$	0
Medium	$-\frac{2}{3}\cdot\frac{T}{a}$	$\frac{2T}{3a}\cdot\frac{1}{3U_{max}^2}$	$-\frac{2}{3}\cdot\frac{T}{a}$	0
Strong	$-\frac{T}{a}$	$\frac{T}{a}\cdot\frac{1}{3U_{max}^2}$	$-\frac{T}{a}$	0

5. Stay cables with nonlinear NSDs

The full-scale stay cable, whose parameters are shown in Table 3, is employed in the numerical analysis in this section. The equivalent stiffness is used in the nonlinear performance evaluation, because it represents the average behavior of a nonlinear NSD when the damper displacement changes from the peak amplitude to zero. The fundamental frequency (ω_1^*) of a stay cable with nonlinear NSD is normalized with respect to the fundamental frequency of a stay cable without control (ω_1^0), and the damping ratio ξ_1 is normalized with respect to $a/2L$ which is commonly regarded as the maximum damping ratio provided by a linear viscous damper to a stay cable.

5.1 Cables with stiffness-hardening NSDs

Fig. 10 shows the frequency variations of the stay cable with nonlinear NSDs showing different degrees of negative stiffness hardening, where the nonlinear NSDs possess pure nonlinear negative stiffness without any damping. The blue, red and green lines represent the cases with weak,

medium and strong nonlinearity in displacement hardening stiffness, respectively. The corresponding parameters are shown in Table 1. The frequencies calculated based on the equivalent stiffness vary slightly with the increasing damper displacement, with the ignorable influence of the stiffness nonlinearity even in the case with strong nonlinearity. The reason is that the equivalent stiffness calculated based on the energy equivalent principles shows the reduced nonlinearity in comparison with the tangent stiffness. In particular, when NSDs are installed close to a cable anchorage, the damper vibration amplitude is typically small.

Figs. 11(a) and 11(b) present the frequencies and damping ratios, respectively, of the stay cables with NSDs possessing both displacement hardening negative stiffness and linear damping coefficients. The damping coefficient is optimized based on the initial tangent stiffness $k_t(0)$ in each case. As shown in Fig. 11(a), adding the viscous damping coefficient further reduces the nonlinearity in the frequencies. Similarly, the damping ratio is hardly affected by the stiffness nonlinearity (Fig. 11(b)).

In general, the displacement hardening stiffness of an NSD imposes limited influences on the dynamic properties of the stay cable. The modal frequencies and damping ratios of the stay cable do not change significantly with the vibration level.

Table 3 Cable parameters

Item	**Value**
Length	122 m
Diameter	11.9 cm
Cross-section area	111 cm2
Young's modulus	$2.0*10^{11}$ N/m^2
Mass	51.8 kg/m
Tension	3150 kN

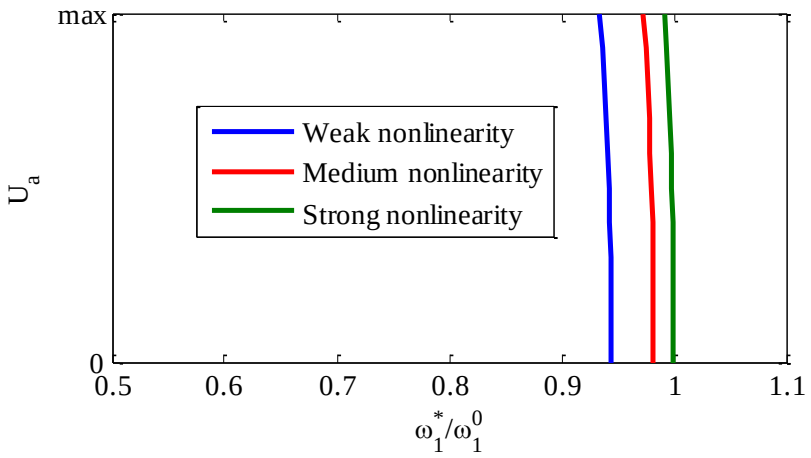

Fig. 10 Variation of frequencies at various vibration amplitude (c=0)

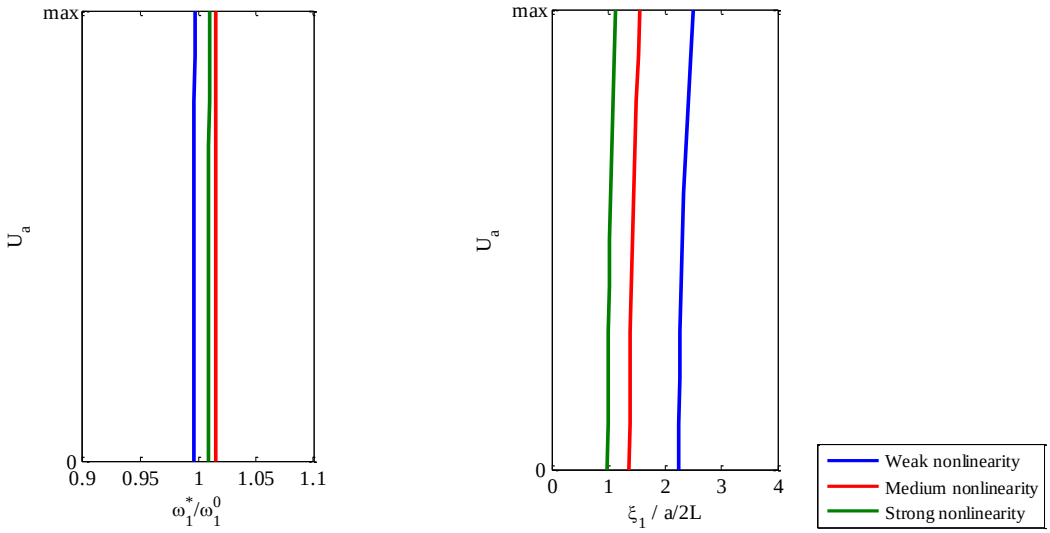

(a) Frequency (b) Damping ratio

Fig. 11 Variation of modal properties at various vibration amplitude (c=c_{opt} for $k_t(0)$)

5.2 Cables with stiffness-softening NSDs

Fig. 12 shows the variation of frequencies of the stay cable with nonlinear NSDs showing different degrees of negative stiffness softening, where the NSD possesses pure nonlinear negative stiffness without any damping. The blue, red and green lines represent the cases with weak, medium and strong softening nonlinearity, respectively. The corresponding parameters are shown in Table 2. As shown in Fig. 12, the cable frequencies calculated based on the equivalent stiffness show limited variation with the increasing damper displacement in the cases of weak and medium cases; the frequency variation is more obvious and within 10% in the case of strong nonlinearity.

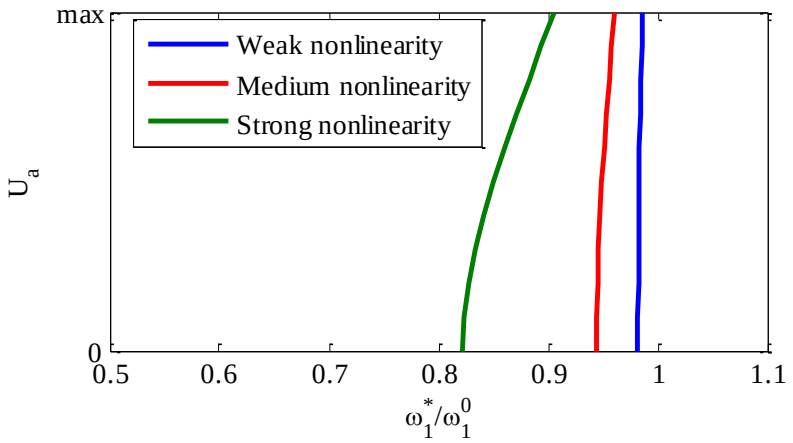

Fig. 12 Variation of frequencies at various vibration amplitude (c=0)

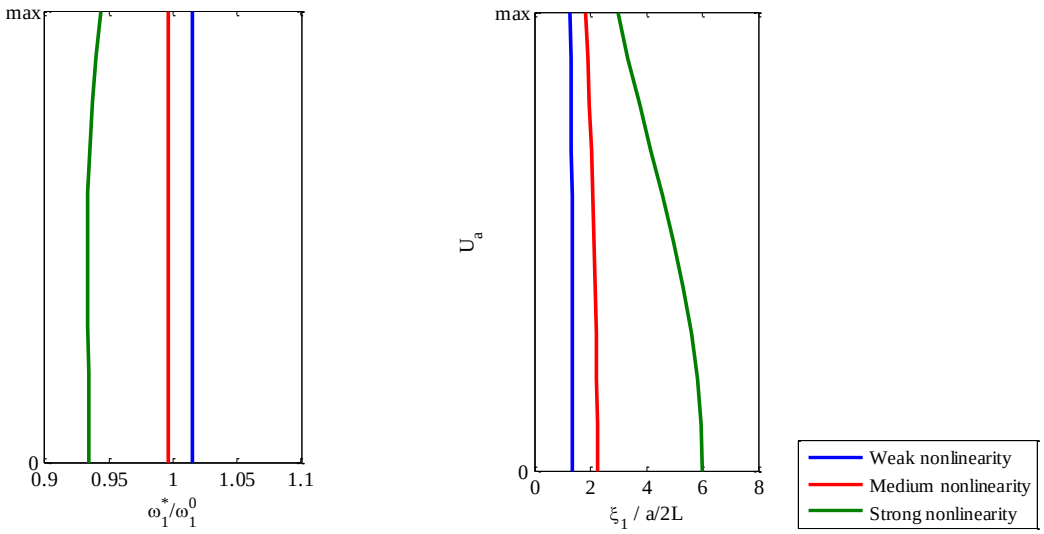

(a) Frequency (b) Damping ratio

Fig. 13 Variation of modal properties at various vibration amplitude (c=copt for $k_t(0)$)

Figs. 13(a) and 13(b) present the frequencies and damping ratios, respectively, of the stay cable with NSDs possessing both displacement softening negative stiffness and linear damping coefficients. The damping coefficients are optimized based on the initial tangent stiffness $k_t(0)$. Again, adding the damping coefficient further reduces the nonlinearity in the modal properties with the increasing vibration amplitude, especially in the cases with the weak and medium nonlinearity of the negative stiffness. Only in the case with the strong nonlinearity in the negative stiffness, the damping ratio of the stay cable degrades with the increasing damper displacement. However, such strong negative stiffness close to the stability limit is not recommended in practical applications.

6. Hilbert transform for nonlinear analysis

To verify the impact of the stiffness nonlinearity of NSD, the dynamic responses of the stay cable with a nonlinear NSD are simulated using the aforementioned state space model in consideration of nonlinear damper stiffness. The vibration time histories will be analyzed through Hilbert Transform (HT). Thus, a brief introduction to Hilbert Transform is provided in this section.

HT is an integral transform firstly introduced by David Hilbert to solve a special case of the integral equations in the area of mathematical physics (Korpel 1982). The HT of the function $x(t)$ is defined as follows (Hahn 1996)

$$H\left[x(t)\right]=\tilde{x}(t)=\pi^{-1}\int_{-\infty}^{\infty}\frac{x(\tau)}{t-\tau}d\tau \tag{28}$$

For vibration analysis, an analytic or quadrature signal is constructed as a complex signal

whose imaginary part as the HT of the real part (Vakman 1998, Lyons 2000). This signal is a two-dimensional signal whose value at some time instant is defined by two parts, namely, the real and imaginary parts (Schreier and Scharf 2010)

$$X(t) = x(t) + i\tilde{x}(t) \tag{29}$$

where $\tilde{x}(t)$ is the HT of $x(t)$. Eq. (29) can also be presented in polar notation (Vainshtein and Vakman 1983)

$$X(t) = |X(t)|\left[\cos\psi(t) + j\sin\psi(t)\right] = A(t)e^{j\psi(t)} \tag{30}$$

where $\psi(t)$ is the instantaneous phase, $\psi(t) = \arctan\dfrac{\tilde{x}(t)}{x(t)}$, and $A(t)$ is the instantaneous amplitude or envelop that can be calculated by

$$A(t) = \sqrt{x^2(t) + \tilde{x}^2(t)} \tag{31}$$

Then the instantaneous angular frequency $\omega(t)$ of an analytic signal is defined as the first derivative of the instantaneous phase $\psi(t)$ as a function of time (Gabor 1946)

$$\omega(t) = \dot{\psi}(t) \tag{32}$$

With a nonlinear system with viscous damping, the equation of motion can be written as (Feldman 1994)

$$\ddot{x}(t) + 2h_0(A)\dot{x} + \omega_0^2(A)x = 0 \tag{33}$$

where $h_0(A) = c(A)/2m$ is the symmetrical viscous damping characteristics, $\omega_0^2(A) = k(A)/m$ is the undamped natural frequency, m is the mass of the system and $k(A)$ is the symmetric elastic characteristics of the system.

By applying the HT to both sides of Eq. (33), multiplying each side of the obtained new equation by i and adding it to Eq. (33), a differential equation for the analytical signal $X(t)$ can be obtained (Feldman 1994)

$$\ddot{X}(t) + 2h_0(A)\dot{X} + \omega_0^2(A)X = 0 \tag{34}$$

where the first and second derivatives of the analytical signal are

$$\begin{aligned}\dot{X} &= X(t)\left[\dot{A}(t)/A(t) + i\omega(t)\right]\\ \ddot{X} &= X(t)\left[\ddot{A}(t)/A(t) - \omega^2(t) + 2i\dot{A}(t)\omega(t)/A(t) + i\dot{\omega}(t)\right]\end{aligned} \tag{35}$$

Substituting Eq. (35) into Eq. (34) yields (Feldman 1994)

$$X\left[\frac{\ddot{A}}{A} - \omega^2 + \omega_0^2 + 2h_0\frac{\dot{A}}{A} + i\left(2\frac{\dot{A}}{A}\omega + \dot{\omega} + 2h_0\omega\right)\right] = 0 \tag{36}$$

where A and ω are the envelope and instantaneous frequency, respectively.

By solving the real and imaginary parts of Eq. (36), the instantaneous modal parameters of the system can be calculated based on the signal envelope and instantaneous frequency (Feldman 1994)

$$\begin{aligned} \omega_0^2(t) &= \omega^2 - \frac{\ddot{A}}{A} + \frac{2\dot{A}^2}{A^2} + \frac{\dot{A}\dot{\omega}}{A\omega} \\ h_0(t) &= -\frac{\dot{A}}{A} - \frac{\dot{\omega}}{2\omega} \end{aligned} \tag{37}$$

By integrating the instantaneous natural frequency in a given period, the average natural frequency can be calculated by (Feldman 2011)

$$\bar{\omega}^2 = T^{-1}\int_0^T \omega_0^2(t)dt \tag{38}$$

The nonlinear backbone (skeleton) curve can be plotted by the variation of an average natural frequency with the changing amplitude. This curve depicts the natural frequency as a function of a free vibration envelope, so it constitutes an inherent feature of nonlinear systems showing that the oscillation frequency is amplitude dependent.

Feldman (1997) also proposed the frequency response function (FRF) of a nonlinear system by assuming that a harmonic force is applied as the input in the specified frequency range. The FRF of the nonlinear system can be written as

$$A = \left[2A_{\max}h_0(A)\right] / \left\{\omega_0(A)\sqrt{\left[1-\frac{\omega^2}{\omega_0^2(A)}\right]^2 + \frac{4h_0^2(A)\omega^2}{\omega_0^2(A)}}\right\} \tag{39}$$

or in another form

$$\begin{aligned} \omega^2 &= \omega_0^2(A) - 2h_0^2(A) \pm 2\omega_0(A)h_0(A)\sqrt{\frac{A_{\max}^2}{A} - 1 + \frac{h_0^2(A)}{\omega_0^2(A)}} \\ 0 \le A &\le A_{\max}\left[1-\frac{h_0^2(A)}{\omega_0^2(A)}\right]^{-1/2} \end{aligned} \tag{40}$$

where A_{max} is the maximum vibration amplitude, ω is the angular frequency of the vibration.

7. Numerical validation of nonlinear stiffness impact

7.1 Dynamic simulation

The full-scale stay cable described in Table 3 is simulated as a numerical example. The cable is discretized into 100 uniformly spaced segments with 99 internal nodes. The nonlinear tangent stiffness k_t can be calculated based on the damper displacement at any instant, and then stiffness matrix **K** and state matrix **A** can be updated in each time step. The NSDs with both displacement

hardening and softening stiffness behaviors are simulated. The damper parameters in the two cases are presented in Table 4. The damping coefficients are the optimal values for initial tangent stiffness $k_t(0)$. The dynamic responses of the stay cable with different passive nonlinear NSDs can be obtained through the state space method. The free vibration responses at the middle span of the stay cable are presented in Figs. 14 and 15 for the stiffness hardening and softening cases, respectively.

Based on the free vibration time histories presented in Figs. 14 and 15, the modal properties of the stay cable with a nonlinear NSD can be analyzed via the HT. Compared with the displacement hardening stiffness case, the responses from the displacement softening stiffness cases decay much faster (Figs. 14 and 15). The first term α_1 (i.e., the linear term) has the largest weights in equivalent stiffness (as shown in Eq. (25)), and the second term describes the nonlinear degree. The equivalent negative stiffness in the softening case is greater, although the nonlinearity degrees in both cases are similar.

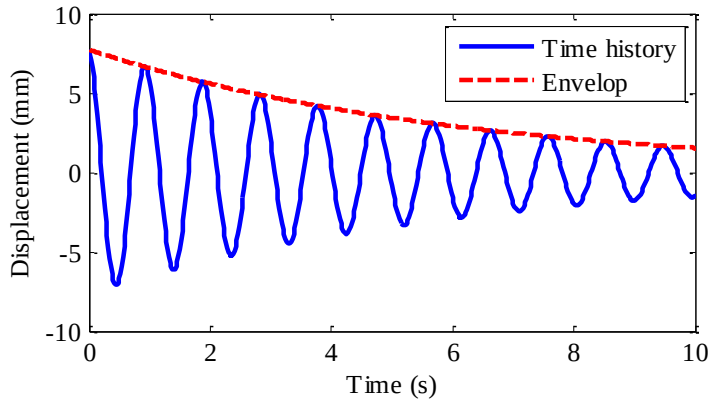

Fig. 14 Free vibration response at the middle span of the stay cable in the hardening stiffness case

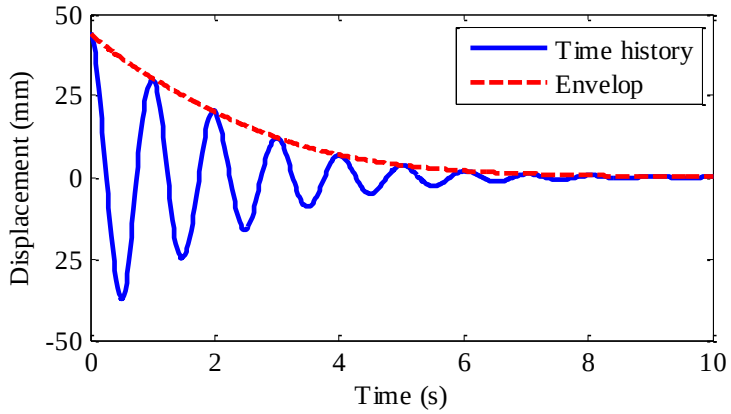

Fig. 15 Free vibration response at the middle span of the stay cable in the softening stiffness case

Table 4 Damper parameters of dynamic simulation

Case No.	Displacement hardening stiffness	Displacement softening stiffness
α_1 (N/m)	0	-464750
α_3 (N/m^3)	-1.55*10^9	1.55*10^9
k_t(0)(T/a)	0	-0.9
k_t(10mm) (T/a)	-0.9	0
c (Ns/m)	81900	28700

7.2 HT Analysis

The response of the stay cable in frequency domain can be obtained via the HT of the responses in time domain. With the constructed analytical signal, the instantaneous amplitude and frequency can be calculated based on Eqs. (31) and (32). Finally, the backbones of frequency and damping ratio, and the FRF can be calculated based on Eqs. (39) and (40).

Fig. 16 shows the modal frequencies and FRF of the stay cable in the stiffness hardening case. The modal frequency calculated based on the equivalent stiffness agree well with the backbone obtained from the HT analysis. The results from HT also indicate that the effect of hardening stiffness on the modal frequency of the cable is very limited. Fig. 17 shows the first modal damping ratio of the stay cable in the stiffness hardening case. The modal damping ratio calculated based on the equivalent stiffness is identical to that obtained via HT analysis. The damping performance does not degrade with the variation in the vibration amplitude at the damper location, indicating an ignorable nonlinear effect on the damping performance in this case.

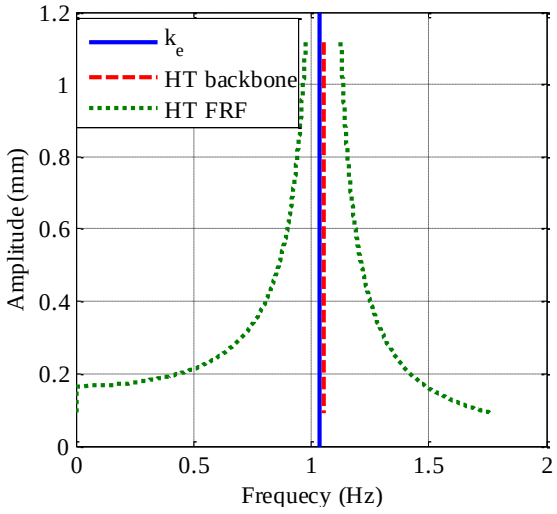

Fig. 16 Modal frequency of stay cable vs. damping vibration amplitude in hardening stiffness case

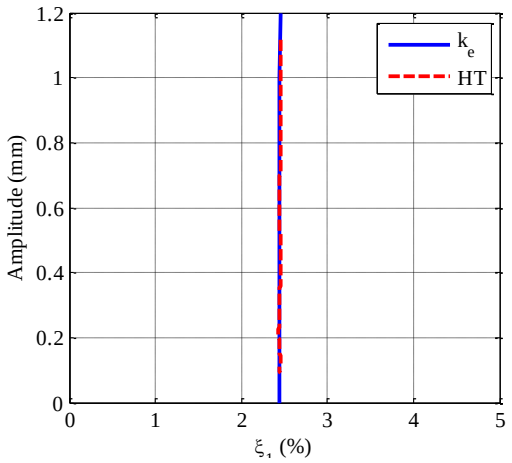

Fig. 17 Damping ratio of stay cable vs. damper vibration amplitude in hardening stiffness case

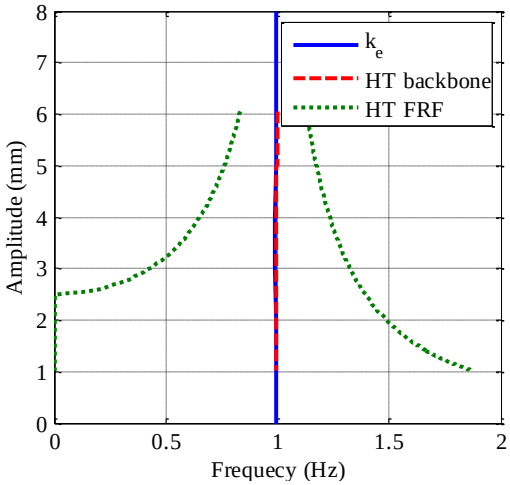

Fig. 18 Modal frequency of stay cable vs. damping vibration amplitude in softening stiffness case

Fig. 18 shows the modal frequencies and FRF of the stay cable in the stiffness softening case. Similarly, the modal frequency calculated based on the equivalent stiffness is very close to that obtained via HT analysis. The effect of stiffness nonlinearity is minimal. Fig. 19 shows the first modal damping ratio of the stay cable in the displacement softening stiffness case. The damping ratios of the stay cable decrease with the increasing damper displacement. The damping ratio calculated based on the equivalent negative stiffness agrees fairly well with the results from the HT analysis, and their discrepancy increases with the vibration displacement. In general, the differences are within 10%, demonstrating that using the equivalent stiffness based on the energy equivalent principle to represent the nonlinear stiffness is an acceptable approach.

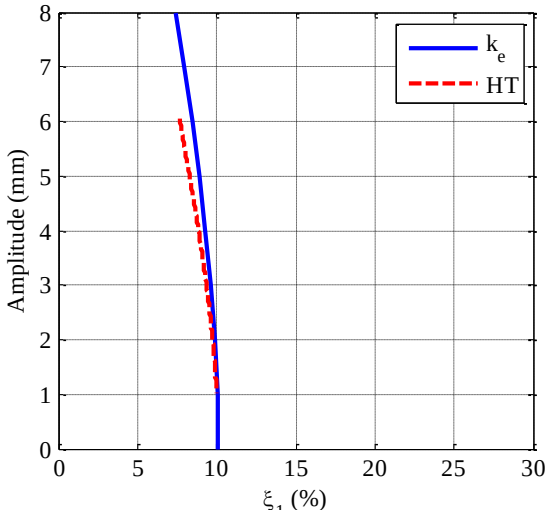

Fig. 19 Damping ratio of stay cable vs. damper vibration amplitude in softening stiffness case

8. Conclusions

This paper investigates the nonlinear stiffness impact of NSDs on the performance of stay cable vibration control. The nonlinear effect from nonlinear negative stiffness is evaluated by the energy equivalent principle. Such linearization weakens the nonlinear effect in the equivalent negative stiffness. Consequently, the influences of the stiffness nonlinearity are quite limited on the vibration mitigation performance in most cases. The accuracy and the conclusions based on the equivalent stiffness is further validated via the HT of the free vibration response of a stay cable with a nonlinear NSD. The modal frequencies and damping ratios of the stay cable can be well predicted by the linearization method. However, it shall be pointed out that the equivalent stiffness using the stiffness linearization approach can only be applied to evaluate the overall damping performance of the nonlinear NSD on stay cable, while the stability issues and instantaneous peak responses shall be analyzed with accurate tangential stiffness.

Acknowledgments

The authors are grateful for the financial supports from the Research Grants Council of Hong Kong through the GRF grant (Project No. PolyU 152222/14E), the Hong Kong Polytechnic University (Project No. 1-ZVJS) and the Innovation and Technology Commission of the HKSAR Government to the Hong Kong Branch of National Rail Transit Electrification and Automation Engineering Technology Research Center (Project No. 1-BBYB). The findings and opinions expressed in this paper are solely those of the authors and not necessarily the views of sponsors.

References

Chen, L., Sun, L. and Nagarajaiah, S. (2015), "Cable with discrete negative stiffness device and viscous damper: passive realization and general characteristics", *Smart Struct. Syst*., **15**(3), 627-643.

Christenson, R.E., Spencer Jr, B.F. and Johnson, E.A. (2006), "Experimental verification of smart cable damping", *J. Eng. Mech*., **132**(3), 268-278.

Feldman, M. (1994), "Non-linear system vibration analysis using Hilbert transform--I. Free vibration analysis method'Freevib'", *Mech. Syst. Signal Pr*., **8**(2), 119-127.

Feldman, M. (1997), "Non-linear free vibration identification via the Hilbert transform", *J. Sound Vib*., **208**(3), 475-489.

Feldman, M. (2011), "Hilbert transform in vibration analysis", *Mech. Syst. Signal Pr*., **25**(3), 735-802.

Fujino, Y. and Hoang, N. (2008), "Design formulas for damping of a stay cable with a damper", *J. Struct. Eng*., **134**(2), 269-278.

Gabor, D. (1946), "Theory of communication. Part 1: The analysis of information. Electrical Engineers-Part III: Radio and Communication Engineering", *J. Institut*., **93**(26), 429-441.

Hahn, S.L. (1996), Hilbert transforms in signal processing. Artech House, 305.

Hoang, N. and Fujino, Y. (2009), "Multi-mode control performance of nonlinear dampers in stay cable vibrations", S*truct. Control Health Monit*., **16**(7-8), 860-868.

Iemura, H. and Pradono, M.H. (2002), "Passive and semi-active seismic response control of a cable-stayed bridge", *J. Struct. Control*, **9**(3), 189-204.

Iemura, H. and Pradono, M.H. (2009), "Advances in the development of pseudo-negative-stiffness dampers for seismic response control", *Struct. Control Health Monit*., **16**(7-8), 784-799.

Johnson, E.A., Christenson, R.E. and Spencer Jr, B.F. (2003), "Semiactive damping of cables with sag", *Comput.-Aided Civil Infrastruct. E*., **18**(2), 132-146.

Korpel, A. (1982), "Gabor: frequency, time, and memory", *Appl. Opt*., **21**(20), 3624-3632.

Kovacs, I. (1982), "Zur frage der seilschwingungen und der seildämpfung", Bautechnik, **59**(10).

Krenk, S. (2000), "Vibrations of a taut cable with an external damper", *J. Appl. Mech*., **67**(4), 772-776.

Krenk, S. and Høgsberg, J.R. (2005), "Damping of cables by a transverse force", *J. Eng. Mech*., **131**(4), 340-348.

Lee, C.M., Goverdovskiy, V.N. and Temnikov, A.I. (2007), "Design of springs with "negative" stiffness to improve vehicle driver vibration isolation", *J. Sound Vib*., **302**(4), 865-874.

Li, H., Liu, M., Ou, J.P. and Guan, X.C. (2005), "Design and analysis of magnetorheological dampers with intelligent control systems for stay cables", Zhongguo Gonglu Xuebao (China J. Highway Transport), **18**(4), 37-41.

Li, H., Liu, M. and Ou, J. (2008), "Negative stiffness characteristics of active and semi-active control systems for stay cables", *Struct. Control Health Monit*., **15**(2), 120-142.

Lyons, R. (2000), Quadrature signals: complex, but not complicated. URL: http://www. dspguru. com/info/tutor/quadsig. htm.

Main, J.A. and Jones, N.P. (2002a), "Free vibrations of taut cable with attached damper. I: Linear viscous damper", *J. Eng. Mech*., **128**(10), 1062-1071.

Main, J.A. and Jones, N.P. (2002b), "Free vibrations of taut cable with attached damper. II: Nonlinear damper", *J. Eng. Mech*., **128**(10), 1072-1081.

Mehrabi, A.B. and Tabatabai, H. (1998), "Unified finite difference formulation for free vibration of cables", *J. Struct. Eng*., **124**(11), 1313-1322.

Nayfeh, A.H. (1979), Nonlinear Oscillations, Wiley-Interscience, s.l., 704.

Ni, Y.Q., Chen, Y., Ko, J.M. and Cao, D.Q. (2002), "Neuro-control of cable vibration using semi-active magneto-rheological dampers", *Eng. Struct*., **24**(3), 295-307.

Pacheco, B.M., Fujino, Y. and Sulekh, A. (1993), "Estimation curve for modal damping in stay cables with viscous damper", *J. Struct. Eng*., **119**(6), 1961-1979.

Pasala, D.T.R., Sarlis, A.A., Nagarajaiah, S., Reinhorn, A.M., Constantinou, M.C. and Taylor, D. (2013),

"Adaptive negative stiffness: new structural modification approach for seismic protection", *J. Struct. Eng*., **139**(7), 1112-1123.
Schreier, P.J. and Scharf, L.L. (2010), Statistical signal processing of complex-valued data: the theory of improper and noncircular signals, Cambridge University Press.
Shi, X. and Zhu, S. (2015), "Magnetic negative stiffness dampers", *Smart Mater. Struct*., **24**(7), 072002.
Shi, X., Zhu, S., Li, J.Y. and Spencer Jr, B.F. (2016), "Dynamic behavior of stay cables with passive negative stiffness dampers", *Smart Mater. Struct*., **25**(7), 075044.
Shi, X. and Zhu, S. (2017), "Simulation and optimization of magnetic negative stiffness dampers", *Sensor. Actuat. A - Phys*., **259**, 14-33.
Shi, X., Zhu, S. and Spencer Jr, B.F. (2017a), "Experimental study on passive negative stiffness damper for cable vibration mitigation", *J. Eng. Mech*., **143**(9), 04017070.
Shi, X., Zhu, S. and Nagarajaiah, S. (2017b), "Performance comparison between passive negative-stiffness dampers and active control in cable vibration mitigation", J. Bridge Eng., **22**(9), 04017054.
Spencer, B. and Nagarajaiah, S. (2003), "State of the art of structural control", *J. Struct. Eng*., **129**(7), 845-856.
Vakman, D.E. (1998), Signals, oscillations, and waves: a modern approach, Artech House Publishers.
Vainshtein, L.A. and Vakman, D.E. (1983), Frequency Separation in the Theory of Vibration and Waves.Nauka, Moscow, 288
Weber, F. and Boston, C. (2011), "Clipped viscous damping with negative stiffness for semi-active cable damping", *Smart Mater. Struct*., **20**(4), 045007.
Weber, F. and Distl, H. (2015), "Semi-active damping with negative stiffness for multi-mode cable vibration mitigation: approximate collocated control solution", *Smart Mater. Struct*., **24**(11), 115015.
Wu, W.J. and Cai, C.S. (2006), "Experimental study of magnetorheological dampers and application to cable vibration control", *J. Vib. Control*, **12**(1), 67-82.
Yamaguchi, H. and Fujino, Y. (1998), "Stayed cable dynamics and its vibration control", *Bridge Aerod*., 235-254.
Zhou, H.J. and Sun, L.M. (2013), "Damping of stay cable with passive-on magnetorheological dampers: a full-scale test", *Int. J. Civil Eng*., **11**(3), 154-159.
Zhou, P. and Li, H. (2016), "Modeling and control performance of a negative stiffness damper for suppressing stay cable vibrations", *Struct. Control Health Monit*., **23**(4), 764-782.